Progress In Electromagnetics Research, Vol. 120, 387–401, 2011

A NOVEL FAST NEAR-FIELD ELECTROMAGNETIC IMAGING METHOD FOR FULL ROTATION PROBLEM

W. Yan[1,*], J.-D. Xu[1], N.-J. Li[1,2], and W.-X. Tan[3]

[1]School of Electronic and Information, Northwestern Polytechnic University, Xi'an, Shaanxi 710129, China

[2]UAV Specialty Technique Key Laboratory of National Defense Technology, Northwestern Polytechnic University, Xi'an, Shaanxi 710129, China

[3]The National Key Laboratory of Microwave Imaging Technology, Beijing 100080, China

Abstract—A fast method for electromagnetic imaging from monostatic full rotational near-field scattering is proposed in this paper. It is based on circular spectrum theory which exploits the Fourier decomposition of the targets distribution instead of point by point imaging in earlier works. The novelty of the proposed method is that it simplifies the relationship between the spatial frequency domain and the scattering field. The near-field scattering is analyzed by expanding the distance to Taylor series at the centre of the targets zone. The near-field focus function is then transformed to spatial frequency domain and evaluated by the method of stationary phase. The imaging result is given by two-dimensional inverse Fourier transformation from spatial frequency domain of targets. The proposed method is validated by comparing the simulation results of distributed targets with the tomographic imaging. The dynamic range of imaging result is derived by distributed targets with different reflection coefficient. Furthermore, the experiment is also conducted in microwave chamber at Ku band with target placed on the turntable.

Received 4 July 2011, Accepted 23 September 2011, Scheduled 27 September 2011

* Corresponding author: Wei Yan (yanwei_nwpu@163.com).

1. INTRODUCTION

Near-field imaging technologies are currently in strong demand in large variety of fields. In medical sciences, it has been used to acquire structure image for detecting breast tumor and other diseases [1–5]. It has also been employed for far-field RCS prediction with near-field measurement of targets back-scattering properties [6, 7]. The advantageous property of the near-field imaging is that it entails limited space for targets imaging, which will reduce the cost by measuring in far-field requirement. In order, to collect the full angular information of targets, the bi-static measurement around a circular path is needed; however, it is time-consuming to acquire the measured data. If the targets satisfy the single scattering model, the bi-static far-field system can be approximately evaluated by the monostatic near-field system.

In the near-field situation, several fast methods for inverse scattering problems have been developed [10, 11], but those are only limited to small angle rotation situation. For wide angle rotation problem, the expanding of the near field distance is highly complex. Therefore, the imaging process is always performed point by point, such as tomographic algorithm and fast cyclical convolution algorithm. The near-field tomographic algorithm has been used to evaluate the image at Cartesian grid points [6–9] and [18]. The downrange profiles are computed for all angles using an FFT-algorithm with appropriate zero-padding. Later, each grid point is calculated by interpolation from downrange profiles. Although, tomographic method performs the FFT to obtain the downrange profile, it still needs summaries for angular domain. The computational complexity is known as $O(kN^2)$, where $N \times N$ for point by point imaging and k stands for summary at angular domain. Fast cyclical convolution algorithm has also been used in large angular rotation problem [12, 13]. The circular convolution algorithm is used over the azimuth angle which involves the fast calculation. Subsequently, the image at each polar grid point is obtained by summaries at frequency domain. The computational complexity for fast cyclical convolution is also given as $O(kN^2)$, where N^2 for point by point imaging and k for summary at frequency domain.

Recently, circular synthetic aperture radar (CSAR) using circular spectrum theory has been explored for providing the capability of high-resolution images. In CSAR geometry, targets are placed at the centre of circular path while the radar is moving around the track. For this system, a fast algorithm, based on the Fourier decomposition of the Green's function, has been developed earlier for the far-field situation [14–17]. It first transforms the spatial domain of targets

to the spatial frequency domain and performs range compensation to reconstruct the image of SAR targets. However, this method is not accurate when the distance and targets dimensions are comparable.

In this paper, a novel method for the near field circular electromagnetic imaging, based on the Fourier decomposition of the Green's function, is proposed. It is analyzed in spatial frequency domain and transformed to spatial domain. The performance of the proposed method is compared with tomographic imaging algorithm. The two methods are both imaging methods in frequency domain. The tomographic method only relates the scattered field to the image by one dimensional FFT in frequency domain; whereas, the proposed approach obtain the image by relating the scattered field to two dimensional spatial frequency domain. The advantage of proposed method is that it simplifies the relationship between the spatial frequency domain of targets and the scattered field.

In Section 2, the system model is described and imaging techniques is discussed. The resolution and sampling criteria is deduced in Section 3. The imaging steps are given in Section 4 and the interpretation from polar to rectangular spectrum is described. In Section 5, the efficiency of the proposed method is validated by the simulation of the distributed targets. The dynamic range of the image is also shown by another simulation with targets of different scattering intensity. The experiment result with target lying on the turntable is presented in Section 6, followed by our conclusion in Section 7.

2. SYSTEM MODEL

The geometry in cylindrical coordinates of a turntable system is illustrated in Figure 1. A stepped frequency signal is radiated from

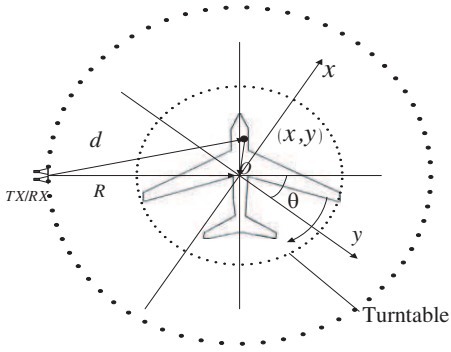

Figure 1. Geometrical parameters of the system.

an antenna, located at the distance R from the centre of the turntable, with an isotropic irradiation to the targets. The reflected signals are received by a similar adjacent antenna which forms a quasi-monostatic system. The targets with reflection coefficient $\psi(x, y)$ are placed on a low reflectivity supporter in the centre of turntable which can rotate around the x-y plane with origin at O. The rotated angle is θ, which stands for the instantaneous position of the turntable. The instantaneous position between the targets and the antenna is d.

2.1. Near-field Scattering

Considering that the antenna is located in the near-field region of the objects, and the amplitude attenuation of the scattering filed is negligible compared to the phase contribution. The scattering electric field of targets in the near-field can be expressed as [10]

$$E_s(f,\theta) = \int_{-\infty}^{\infty}\int_{-\infty}^{\infty} \psi(x,y)\, G(x,y;f,\theta)dxdy \tag{1}$$

where, $G(x, y; f, \theta)$ is near field focus function, which is given by $G(x, y; f, \theta) = e^{-jk\times 2d}$. Here, the wave-number is defined as $k = 2\pi f/c$ and the distance from antenna to the targets is $d = \sqrt{(x - R\cos\theta)^2 + (y - R\sin\theta)^2}$. As the position of targets (x, y) can be expressed as (ρ, ϕ) in polar coordinates, and the distance d can also be given as

$$\begin{aligned} d &= \left|\vec{R} - \vec{\rho}\right| \\ &= \sqrt{R^2 + \rho^2 + 2R\rho\cos(\phi - \theta)} \end{aligned} \tag{2}$$

Since the distance in the near-field is two-dimensional coupling, the problem can not directly resort to two dimensional FFT. A practical method is by expanding the distance into Taylor series. The near-field distance can be expressed by Taylor expansion with different orders. The distance is related to phase of return signals. To keep the phase error within $\pi/8$, the Taylor series of the distance to third order at the targets centre point $\rho = 0$ is given by [9]

$$\begin{aligned} d(\rho) &\approx d(0) - d'(0)\rho + \frac{1}{2!}d''(0)\rho^2 \\ &\approx R - \rho\cos(\theta - \phi) + \frac{\sin^2(\theta - \phi)}{2R}\rho^2 \end{aligned} \tag{3}$$

2.2. Relationship between Near-field Scattering and Spatial Frequency Domain of Targets

According to Parseval's theory, the scattering electric field in (1) can be expressed as

$$E_s(f,\theta) = \int_{-\infty}^{\infty}\int_{-\infty}^{\infty} \psi\left(-k_x,-k_y\right) G\left(k_x,k_y;f,\theta\right) dk_x dk_y \tag{4}$$

where, $\psi\left(-k_x,\ -k_y\right)$ is the spatial frequency domain of targets, and it is given as

$$\begin{aligned}\psi(-k_x,-k_y) &= \int_{-\infty}^{\infty}\int_{-\infty}^{\infty} \psi(-x,-y)\cdot e^{-j[(-k_x(-x)+(-k_y)(-y)]} d(-x)d(-y)\\ &= \mathrm{FFT}_{(-x)}\left(\mathrm{FFT}_{(-y)}\left(\psi\left(-x,-y\right)\right)\right)\end{aligned} \tag{5}$$

The frequency in spatial frequency domain is defined as f', and

$$\begin{aligned} k_x &= \tfrac{4\pi f'}{c}\cos\phi\\ k_y &= \tfrac{4\pi f'}{c}\sin\phi\end{aligned} \tag{6}$$

In (4), $G\left(k_x,\ k_y;\ f,\ \theta\right)$ is the spatial frequency domain of targets, and it is defined as

$$\begin{aligned} G(k_x,k_y;f,\theta) &= \int_{-\infty}^{\infty}\int_{-\infty}^{\infty} G(x,y;f,\theta)e^{-j(k_x x+k_y y)}dk_x dk_y\\ &= \int_{-\infty}^{\infty}\int_{-\infty}^{\infty} e^{-j2kd}e^{-j(k_x x+k_y y)}dk_x dk_y\end{aligned} \tag{7}$$

2.3. Solution of Near Field Focus Function in Spatial Frequency Domain

Since the integrand in (7) has no singular points and is a highly oscillating function, the integral can be evaluated by means of the MSP provided that k is sufficiently large. $(k_x,\ k_y)$ can be expressed as $(k_\rho,\ \phi)$ in polar coordinates. Assuming that the targets position is within the zone: $0 \le \rho \le r$, then

$$k_\rho = \sqrt{k_x^2 + k_y^2} = 2k \tag{8}$$

$$|\phi - \theta| \le \theta_x = a\sin\left({}^{r}/_{R}\right) \tag{9}$$

As k_ρ equals to $4\pi f'/c$, the frequency in spatial frequency domain is given as $f = f'$. The truncation function of the angular sector can be easily assigned by (9).

The spatial frequency domain $G\left(k_x,\, k_y;\, f,\, \theta\right)$ can also be given in polar coordinates as

$$G(k_\rho, \phi; f, \theta) = \int_0^r \int_0^{2\pi} e^{-j2kd} e^{-jk_\rho \rho} \rho d\rho d\phi \tag{10}$$

The phase function within the integral in (10) is

$$\begin{aligned} g(\rho) &= -2kd - k_\rho \rho \\ &\approx -2k\left[R - \rho\cos(\theta-\phi) + \frac{\sin^2(\theta-\phi)}{2R}\rho^2\right] - k_\rho\rho \end{aligned} \tag{11}$$

It can also be expanded as Taylor series at the stationary point

$$g(\rho) \approx g(\rho_0) + g'(\rho_0)(\rho-\rho_0) + g''(\rho_0)\frac{(\rho-\rho_0)^2}{2!} + g'''(\rho_0)\frac{(\rho-\rho_0)^3}{3!} \tag{12}$$

The major contribution to the integral in (10) comes from a small neighborhood near the stationary point $\rho = \rho_0$. According to MSP, the stationary point comes from $g'\left(\rho\right) = 0$, so the stationary point is

$$\rho_0 = R\frac{\cos\left(\theta-\phi\right) - 1}{\sin\left(\theta-\phi\right)} \tag{13}$$

The each order derivative at the stationary point is as follows:

$$\begin{aligned} g(\rho_0) &= -\left[R - \rho_0\cos(\theta-\phi) + \frac{\sin^2(\theta-\phi)}{2R}\rho_0^2 + \rho_0\right] \\ &= -R\left[1 - \frac{1}{2}\tan^2\left(\frac{\theta-\phi}{2}\right)\right] \end{aligned} \tag{14a}$$

$$g'(\rho_0) = 0 \tag{14b}$$

$$g''(\rho_0) = -\frac{\sin^2(\theta-\phi)}{R} \tag{14c}$$

$$g'''(\rho_0) = 1 \tag{14d}$$

In the neighborhood of stationary point $\rho = \rho_0$, the first order derivative $g'\left(\rho_0\right) = 0$ and the second order derivative $g''\left(\rho_0\right)$ vanishes, so

$$g(\rho) \approx g(\rho_0) + g'''(\rho_0)\frac{(\rho-\rho_0)^3}{3!} \tag{15}$$

Substituting $g(\rho)$ with this series expansion, the integral in (10) can be expressed in terms of the Airy function, leading to

$$\begin{aligned} G(k_\rho, \phi; f, \theta) &\approx 2\pi e^{-j2k_0R\left[1-\frac{1}{2}\tan^2\left(\frac{\theta-\phi}{2}\right)\right]} 2^{\frac{1}{3}} Ai(0) \\ &\approx 2.81 e^{-j2k_0R\left[1-\frac{1}{2}\tan^2\left(\frac{\theta-\phi}{2}\right)\right]} \end{aligned} \tag{16}$$

2.4. Interpretation to Obtain the Image of Targets

According to (4) and (16), the scattering electric field becomes

$$\begin{aligned} E_s(f,\theta) &= \int_{-\infty}^{\infty}\int_{-\infty}^{\infty} 2k\psi(k_\rho,\phi)G(k_\rho,\phi;f,\theta)dk_\rho d\phi \\ &= \int_{-\infty}^{\infty}\int_{-\infty}^{\infty} 5.62k\psi(k_\rho,\phi)e^{-j2k_0R\left[1-\frac{1}{2}\tan^2\left(\frac{\theta-\phi}{2}\right)\right]}dk_\rho d\phi \end{aligned} \tag{17}$$

Therefore, the scattering pattern is as follows

$$\psi(k_\rho,\phi) = \frac{1}{5.62}\int_0^{2\pi}\int_{f_{\min}}^{f_{\max}} \frac{E_s(f,\theta)}{k} e^{j2k_0R\left[1-\frac{1}{2}\tan^2\left(\frac{\theta-\phi}{2}\right)\right]} df d\theta \tag{18}$$

The polar samples of $\psi(k_\rho, \phi)$ are then converted to the samples of $\psi(-k_x, -k_y)$, where

$$\begin{aligned} k_x(f,\theta) &= -2k_\rho\cos\phi \\ k_y(f,\theta) &= -2k_\rho\sin\phi \end{aligned} \tag{19}$$

Via bi-linear interpolation algorithm, the rectangular spectrum of targets $\psi(-k_x, -k_y)$ is calculated. The 2-D inverse Fourier transform of this signal is the rotation by π of desired image $\psi(x, y)$. The computation complexity is mainly from two-dimensional summaries for $\psi(k_\rho, \phi)$ in (18) and is $O(N^2)$.

3. RESOLUTION AND SAMPLING CRITERIA

The proposed method is an image-based method for monostatic near field imaging, therefore, it is only suited for single scattering model, however, cannot address the complex targets due creeping wave or coupling.

The resolution limit depends on centre lobe of point spread function (PSF). As the frequency vary from $f_{\min}$ to $f_{\max}$, the spatial domain of targets k_ρ is constrained in $[k_{\rho_{\min}}, k_{\rho_{\max}}]$ Assuming that

the object is a reflecting point placed at the origin, the point spread function can be expressed as

$$\mathrm{PSF}\,(x,y) = k_{\rho_{\max}} \frac{J_1\left(\rho k_{\rho_{\max}}\right)}{\rho} - k_{\rho_{\min}} \frac{J_1\left(\rho k_{\rho_{\min}}\right)}{\rho} \tag{20}$$

J_1 is the Bessel function of the first order. In the extreme case of $k_{\rho_{\min}} = 0$, the radial resolution becomes $\delta x = \delta y = \frac{\pi}{k_{\rho_{\max}}}$.

Assuming the object is confined within a circular zone $0 \le \rho \le r$, the sampling intervals needed to satisfy the Nyquist criterion. In the frequency domain, the frequency step is given by

$$\Delta f \le c/\left(4r\right) \tag{21}$$

In the angular domain, it requires that the angular increments be sufficiently small to make the phase of signals vary less than π radians between samples. As the maximum phase of targets for an angular increment $\Delta\theta$ is $k_{\rho_{\min}} r \sin(\Delta\theta)$, the angular step can be given as

$$\Delta\theta \le a \sin\left[\lambda_{\min}/\left(4r\right)\right] \tag{22}$$

4. THE STEPS OF IMAGING

Following are the steps devised for proposed imaging:

1) Compute the spatial frequency domain of near field focus function $G\left(k_\rho,\, \phi;\, f,\, \theta\right)$ at the sample points according to (18);
2) Compute $\psi\left(k_\rho,\, \phi\right)$ according to (18) and (20);
3) Use polar to rectangular interpolation to reconstruct $\psi\left(-k_x,\, -k_y\right)$ from the polar data as follows:
   a) The occupying rectangular zone of polar spectrum is obtained and chosen as edge of rectangular spectrum as shown in Figure 2. The polar spectrum is shown as solid points, while the required rectangular spectrum is hollow points;
   b) The 2D k_x and k_y intervals should be chosen same as the intervals of k_ρ;
   c) Bi-linear interpolation algorithm should be used for two dimensional interpolations from polar grid points to rectangular grid points;
4) Perform the inverse FFT transformation to acquire $\psi\left(-x,\, -y\right)$;
5) Rotate the $\psi\left(-x,\, -y\right)$ by π to obtain the targets image $\psi\left(x,\, y\right)$.

5. SIMULATION RESULTS

In this section, the performance of the proposed fast near-field imaging method implemented with circular spectrum approach is illustrated with comparison to the near-field tomographic method. The tomographic method was first used in the medical imaging, and later introduced to extract the target shape information from circular path data in the reference [18]. It first divides the image zone into $N \times N$ grid points, and then calculates the amplitude and phase for each point.

The frequency range of the following examples is $f = 8 \sim 12\,\text{GHz}$ with 401 frequency steps, the angular aperture is $\theta = 0^\circ$ to 360° with 1201 angular steps. The near-field distance R is 5 m. The targets geometry with same reflectivity 0 dBsm is shown in Figure 3(a), which is used to construct the letter 'E' and 'M'. The far-field is defined as $2D^2/\lambda$. The targets dimension D is about 1.2 m, so the far-field is 115.2 m. The near field distance is within 5% of far field requirement. The resolution corresponding to the above parameters is 0.01 m. The forward solver for synthetic data without noise is based on integrating the contribution of each scatterer which can be found in the reference [4] and [10]. The spatial frequency domain $\psi(k_x, k_y)$ of the targets is given in Figure 3(b). It is obtained by 2-D bi-linear interpretation from $\psi(k_\rho, \phi)$. As k_ρ is within the zone $[k_{\rho_{\min}}, k_{\rho_{\max}}]$, $\psi(k_x, k_y)$ in rectangular coordinate system forms a ring. The image result by proposed method is given in Figure 3(c), by performing the 2-D inverse FFT from $\psi(k_x, k_y)$. From Figure 3(c), the two targets with distance 0.05 m in letter 'M' are clearly distinguished. It shows that the proposed method has resolution higher than 0.05 m. Figure 3(d) is the result by tomographic method. It is found that the result by proposed method can provide accurate image with the shape of targets

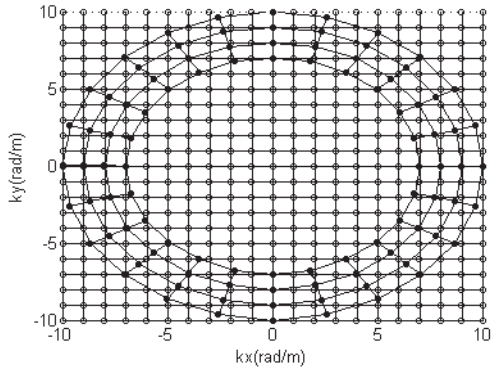

Figure 2. Interpolation in spectrum domain.

kept. The processing time by proposed method in this paper is 25.94 s, whereas in tomographic method the same processing takes 1043.93 s. The efficiency of proposed method appears from analyzing in spatial frequency and evaluation by MSP for near field focus function.

In order to assure accurate reconstruction, reasonable sampling point number should be defined for the system. In the previous simulation, the target is within a circular zone $0 \leq \rho \leq r = 1\,\mathrm{m}$, so the criteria of angular steps and frequencies can be obtained by the formula in Section 3:

$$\Delta f \leq c/(4r) = c/4 = 0.075\,\mathrm{GHz} \tag{23}$$

$$\Delta\theta \leq a\sin\left[\lambda_{\min}/(4r)\right] = a\sin\left[c/(4rf_{\min})\right] = 0.358^{\circ} \tag{24}$$

In order to show the influence of steps reduction, simulation is performed with different angular steps and frequencies. In Figure 4(a), the angular steps and frequencies is 0.3 degree and 0.01 GHz, which is

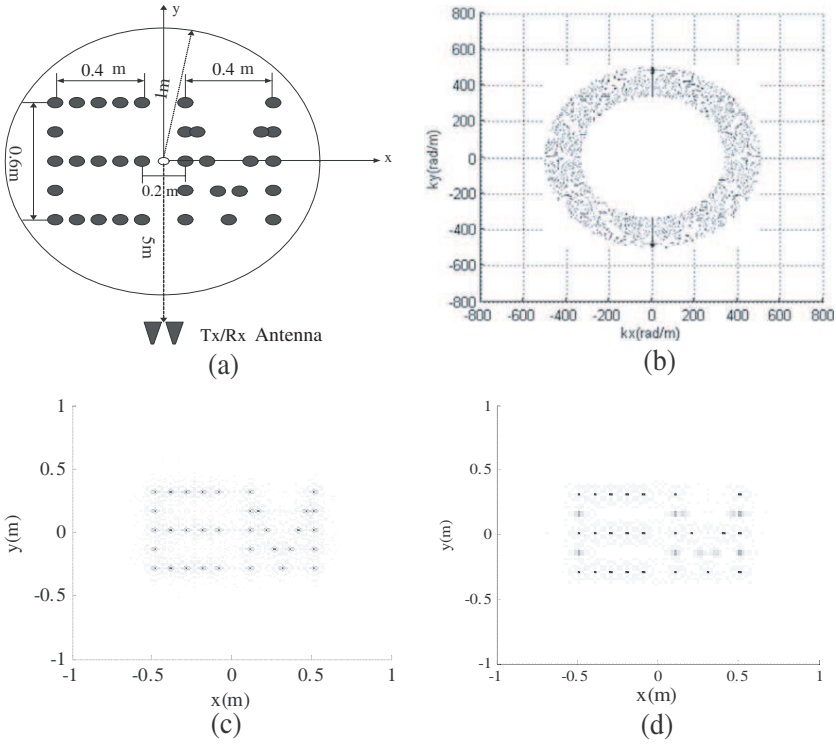

Figure 3. Simulation model and results. (a) Targets model. (b) Spectrum of targets image. (c) Targets' image by proposed method. (d) Targets' image by tomographic method.

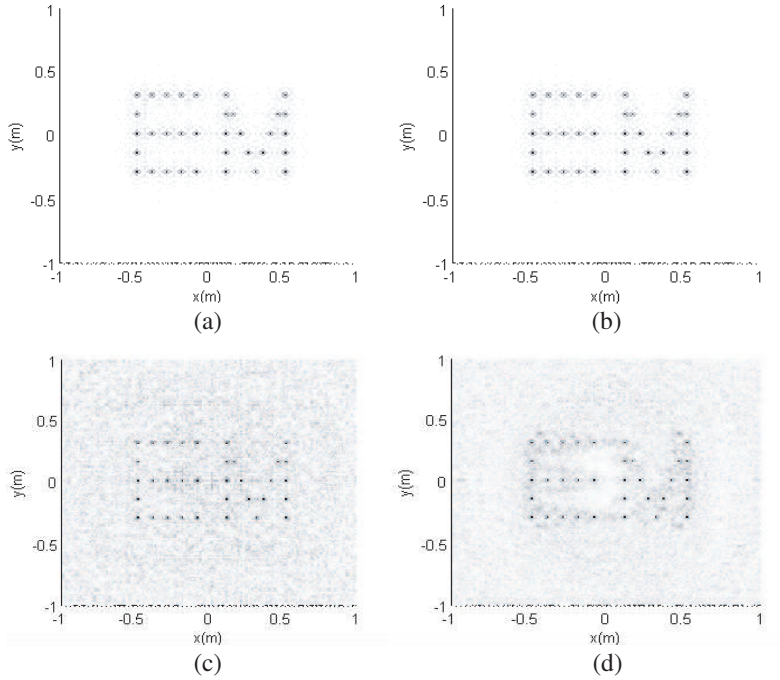

Figure 4. Targets image by proposed method with different sampling intervals. (a) $\Delta\theta = 0.3^\circ$ $\Delta f = 0.01\,\text{GHz}$. (b) $\Delta\theta = 0.3^\circ$ $\Delta f = 0.05\,\text{GHz}$. (c) $\Delta\theta = 16^\circ$ $\Delta f = 0.01\,\text{GHz}$. (d) $\Delta\theta = 0.3^\circ$ $\Delta f = 0.2\,\text{GHz}$.

oversampled. In Figure 4(b), the angular steps and frequencies are 0.3 degree and 0.05 GHz, which is near the criteria. The angular steps and frequencies in Figure 4(c) is 1 degree and 0.05 GHz, which is not satisfying the criteria in angular domain. The angular steps and frequencies in Figure 4(d) is 0.3 degree and 0.2 GHz, which does not satisfy the criteria in frequency domain. The comparisons show that if the criteria are not satisfied, the image is blurred and can not reflect the required targets information. However, when the angular steps and frequencies are oversampled, experimental as well as the image processing time would become long. The reason leading to distortion of image is caused by the phase of signals which vary over π radians between the samples.

To show the dynamic range of image, simulation with targets of different reflection coefficient is setup. The frequency band of the following examples at X band from $8 \sim 12\,\text{GHz}$, with 401 frequency sampling points, the angular aperture is $\theta = 0^\circ$ to 360° with 361 angular steps. The near-field distance R is 5 m. The targets geometry

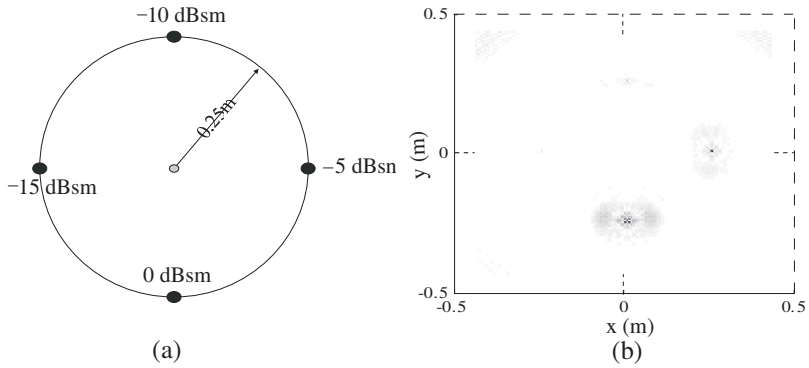

Figure 5. Simulation model and result. (a) Targets model. (b) Targets image by proposed method.

is shown in Figure 5(a), with the largest size D equal to 0.5 m. The result in Figure 5(b) by proposed method shows that the dynamic range of the image is about 15 dB. The proposed method is useful when the targets with large dynamic range are placed not too close. If a target with small reflectivity is placed near a target with high reflectivity, it may not be distinguished due to the side lobe influence of the high reflectivity target.

6. EXPERIMENTAL RESULTS

The experiment was performed in microwave chamber with dimension 15 m×15 m×25 m. The step frequency signal is generated by an Agilent Vector Network Analyzer 8363A. The received signal is also captured by Vector Network Analyzer but with different ports. The transmitting antenna and receiving antenna are standard horn antennas which can work at 12 $\sim$ 18 GHz. In order to collect scattering data in the experiment, two transmit antennas and two receive antennas are placed on the supporter, as shown in Figure 6(a). Isolation materials are placed between those antennas to avoid coupling. Four antennas are used to measure the four polarization cases, such as HH, HV, VH and VV. To validate the proposed algorithm, only HH polarization is used for imaging and the polarization diversity is not taken in to account.

Target is laid on a low scattering reflection supporter made of foam, as shown in Figure 6(b). Two metallic spheres with radius 5 cm are placed in each hand of the target. Two small metallic adhesive tapes are also stuck on the coat along waist line of the target. The radius of foam supporter is about 1 meter, and it can rotate at 0.01

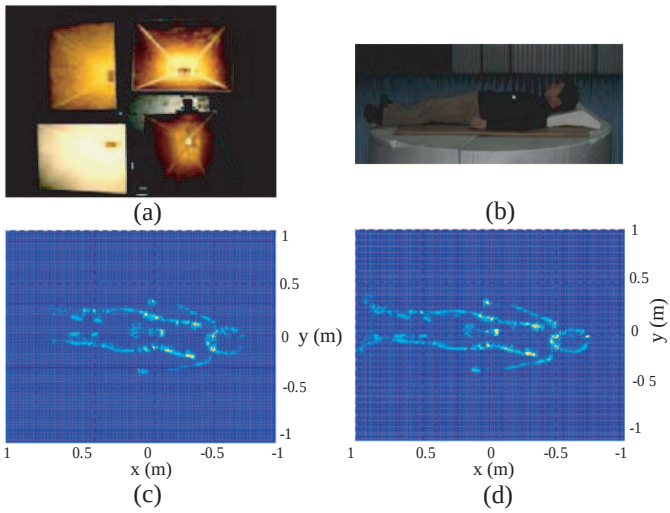

Figure 6. Experimental setup and results. (a) Setup of antennas. (b) The targets on the turntable. (c) Targets image by proposed method. (d) Targets image by tomographic method.

degree angular intervals. The distance between the center of supporter and the antenna is about 19 m. According to far-field requirements, this distance should be over 480 m. Clearly, the target is in the near field zone, which is only about 4% of far-field criterion. The transmitting and receiving antennas were placed very near compared to the measured distance, so it forms a quasi-monostatic system.

The measurement data is obtained with the rotation of the turntable. The frequency sample is 1201 and an angular sample is 1201. The total rotated angle is 360 degree. The imaging result of proposed method is shown in Figure 6(c), while the result by tomographic method is displayed in Figure 6(d). The comparison of these results shows that the proposed method reveals most targets information. In the provided examples, the sampling point number is larger than the sampling criteria to obtain the high image quality of targets. If the angular steps and frequencies are reduced, some details of targets would not exist in the image. The comparison of the results shows that the proposed method has the same accuracy but needs less processing time.

7. CONCLUSION

This paper proposed a fast method predicting the targets image from monostatic near-field scattering. It improves the efficiency of

computation of tomographic methods by analyzing in spatial frequency domain and evaluating the spectrum of near field focus function using MSP. The simulation results show that the proposed method works very well even when the near-field measurement distance is shortened to only 5 percent of the far-field requirements. The experiment is also performed which shows the accuracy of the proposed method. At this stage, it is foreseen that the presented theory of circular spectrum can be extended to the 3D scattering problems.

ACKNOWLEDGMENT

The authors would like to thank the anonymous reviewers for providing a number of important comments and suggestions. This work is supported by the Natural Science Basic Research Plan in Shaanxi Province of China (Grant No.2009JM8001-2) and by NPU Foundation for Fundamental Research (Grant No. NPU-FFR-JC201039) of China.

REFERENCES

1. Zhou, H., T. Takenaka, J. Johnson, and T. Tanaka, "A breast imaging model using microwaves and a time domain three dimensional reconstruction method," *Progress In Electromagnetics Research*, Vol. 93, 57–70, 2009.
2. Yu, J., M. Yuan, and Q. H. Liu, "A wideband half oval patch antenna for breast imaging," *Progress In Electromagnetics Research*, Vol. 98, 1–13, 2009.
3. Zhang, H., S. Y. Tan, and H. S. Tan, "A flanged parallel-plate waveguide probe for microwave imaging of tumors," *Progress In Electromagnetics Research*, Vol. 97, 45–60, 2009.
4. Catapano, I., L. Di Donato, L. Crocco, O. M. Bucci, A. F. Morabito, T. Isernia, and R. Massa, "On quantitative microwave tomography of female breast," *Progress In Electromagnetics Research*, Vol. 97, 75–93, 2009.
5. Chen, G. P. and Z. Q. Zhao, "Ultrasound tomography-guide TRM technique for breast tumor detecting in MITAT system," *Journal of Electromagnetic Waves and Application*, Vol. 24, Nos. 11–12, 1459–1471, 2010.
6. Vaupel, T. and T. F. Eibert, "Comparison and application of near-field ISAR imaging techniques for far-field radar cross section determination," *IEEE Transactions on Antennas and Propagation*, Vol. 54, No. 1, 144–151, 2006.

7. Nicholson, K. J. and C. H. Wang, "Improved near-field radar cross-section measurement technique," *IEEE Antennas and Wireless Propagation Letters*, Vol. 8, 1103–1106, 2009.
8. Tan, W.-X., Y.-P. Wang, W. Hong, Y.-R. Wu, N.-J. Li, C.-F. Hu, and L.-X. Zhang, "Circular SAR experiment for human body imaging," *1st Asian and Pacific Conference on.Synthetic Aperture Radar*, 2007.
9. Tan, W., W. Hong, Y. Wang, and Y. Wu, "A novel spherical-wave three-dimensional imaging algorithm for microwave cylindrical scanning geometries," *Progress In Electromagnetics Research*, Vol. 111, 43–70, 2011
10. Li, S. Y., H. J. Sun, B. C. Zhu, and R. Liu, "Two-dimensional NUFFT-based algorithm for fast near-field imaging," *IEEE Antennas and Wireless Propagation Letters*, Vol. 9, 814–817, 2010.
11. Park, J.-I. and K.-T. Kim, "A comparative study on isar imaging algorithms for radar target identification," *Progress In Electromagnetics Research*, Vol. 108, 155–175, 2010.
12. Broquetas, A., J. Palau, L. Jofre, and A. Cardama, "Spherical wave near-field imaging and radar cross-section measurement," *IEEE Transactions on Antennas and Propagation*, Vol. 45, No. 5, 730–735, 1998.
13. Fortuny, J, "An efficient 3-D near-field ISAR algorithm," *IEEE Transactions on Aerospace and Electronic Systems*, Vol. 34, No. 4, 1261–1270, 1998.
14. Soumekh, M., "Reconnaissance with slant plane circular SAR imaging," *IEEE Transactions on Image Processing*, Vol. 8, No. 8, 1252–1265, 1996.
15. Bryant, M. L., L. L. Gostin, and M. Soumekh, "3-D E-CSAR imaging of a T-72 tank and synthesis of its SAR reconstructions," *IEEE Transactions on Aerospace and Electronic Systems*, Vol. 39, No. 1, 211–227, 2003.
16. Burki, J. and C. F. Barnes, "Slant plane CSAR processing using householder transform," *IEEE Transactions on Image Processing*, Vol. 17, No. 10, 1900–1907, 2009.
17. Lin, Y., W. Hong, W. Tan, and Y. Wu, "Extension of range migration algorithm to squint circular SAR imaging," *IEEE Geoscience and Remote Sensing Letters*, Vol. 8, No. 4, 651–655, 2011.
18. Knaell, K. K. and G. P. Cardillo, "Radar tomography for the generation of three-dimensional images," *IEE Proceedings of Radar, Sonar and Navigation*, Vol. 142, No. 2, 54–60, 1995.